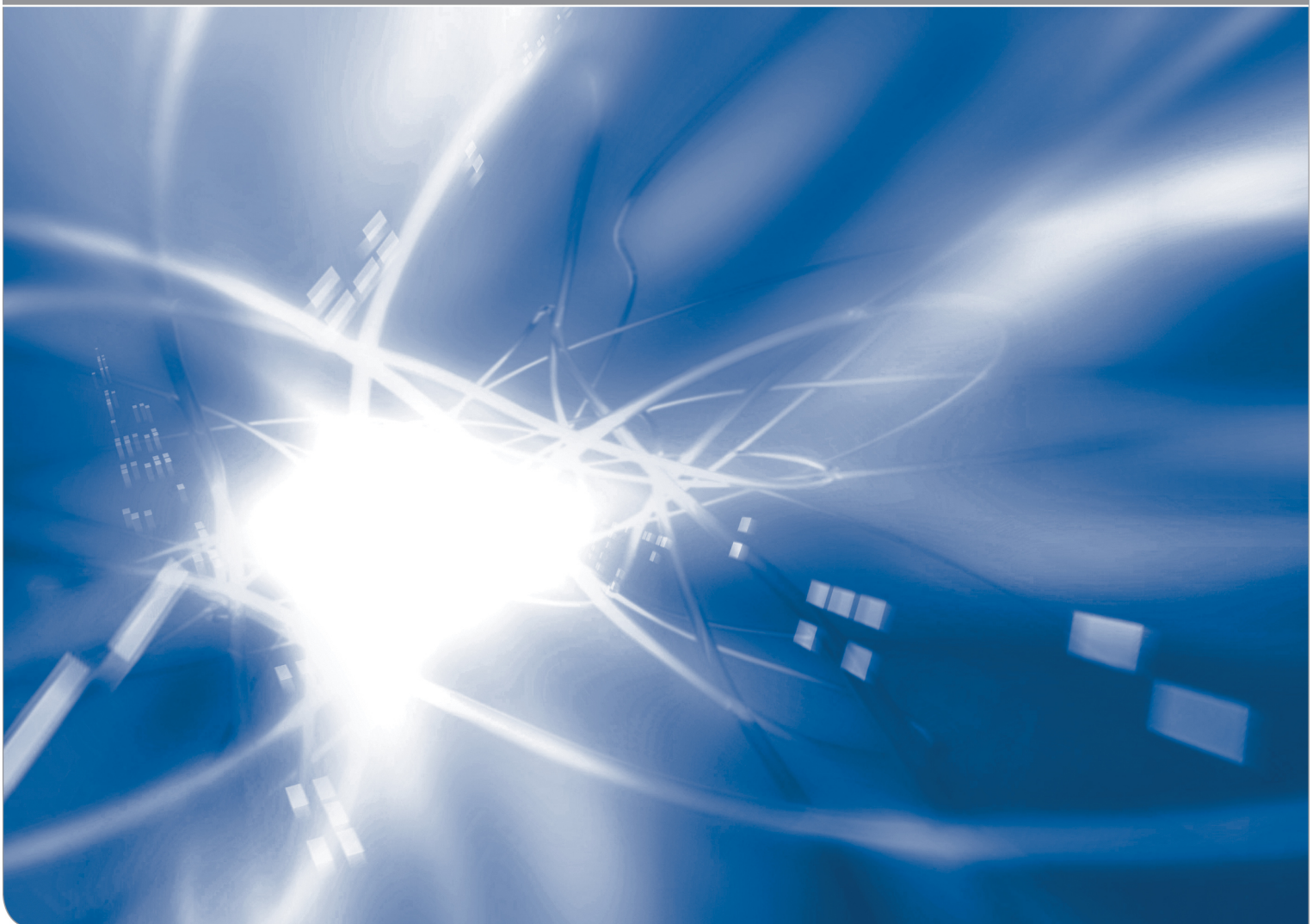# Anomalous temperature behaviour of subcritical crack growth in silica

T. Fett, E.C. Bucharsky, K.G. Schell

KIT SCIENTIFIC WORKING PAPERS 131

IAM Institute for Applied Materials

Impressum

Karlsruher Institut für Technologie (KIT)
www.kit.edu

2019

Abstract

Silica shows the effect of subcritical crack growth in humid environments. Measurements in liquid water show increasing subcritical crack growth velocities when the temperature is increased as was shown by Wiederhorn and Bolz. Since this has been generally found for glasses, this effect is called *normal subcritical crack growth*.

For measurements on silica in water vapour environment the astonishing effect of decreasing crack-growth rate v at an increased temperature was observed for constant partial water pressure in the humid environment. This surprising result observed in v-K experiments by Suratwala and Steele is called *anomalous subcritical crack growth* behavior.

In the present report we consider the effects of reduced water concentration at silica surfaces and volume swelling by hydroxyl generation as the reasons for anomalous subcritical crack growth.

From our computation, we can conclude that silica shows normal subcritical crack growth, when it is taken into account that the real physical stress intensity factor K_I is used that describes the stresses in the singular crack-tip field, i.e. when v-is plotted vs. K_{tip}.

Contents

1 Introduction

Similar as other glasses, also silica shows the effect of subcritical crack growth. Its basic effect bond-break events need very high stresses which are available for sharp cracks only in the singular stress field at crack-tip distances in the order of a few molucule diameters. Crack growth in silica glass has been well described by fracture mechanics techniques representing the mechanical load by the stress intensity factor.

Subcritical crack growth behavior of silica is usually presented in form of $v(K)$-curves where v is the crack-growth rate and K the externally applied stress intensity factor. Results are reported as a function of relative humidity and temperature in [1, 2, 3, 4]. For the description in the temperature range $T \leq 450°C$ very often exponential expressions are used of the form [5]

$$v = A_1 \, p \exp\left[\frac{-Q + bK}{RT}\right] \tag{1}$$

In [6] Wiederhorn et al. suggest

$$v = A_3 [H_2O] k_r(T) \exp\left[\frac{-Q + bK}{RT}\right] \tag{2}$$

In (2) the quantity $k_r(T)$ is the rate coefficient for the single-step reaction showing the temperature dependency

$$k_r(T) \propto T \exp\left[\frac{-\Delta G}{RT}\right] \tag{3}$$

(ΔG=free energy of activation). In order to achieve sufficient transparency, we have simplified the rate coefficient in the Discussion Section equal to $k_r(T)=1$.

For silica the astonishing effect of decreasing crack-growth rate v at an increased temperature was observed for constant partial water pressure in the humid environment. This surprising result observed in v-K experiments by Suratwala and Steele [7] is called *anomalous subcritical crack growth* behavior. A comparison for different glasses is given in Fig. 1. Whereas for silica the crack velocity decreases with temperature, it increases for all other glasses [7]. This conclusion is of course somewhat problematic since curves (1) and (2) are not for silicate glass and curves (3-6) obtained in vacuum cannot describe any influence that water might have. In addition, it is mentioned in [2] that silica in the vacuum tests failed not before toughness was reached. This implies a very steep v-K-curve and consequently subcritical crack growth at a value of $K=0.8$ K_{Ic} could simply not be reached.

Suratwala and Steele [7] assume that the negative temperature dependence will stem from a change in the slow crack growth resistance of the glass upon exposure to temperature and stress. In the following considerations we will try to explain the effect by a simpler reason.
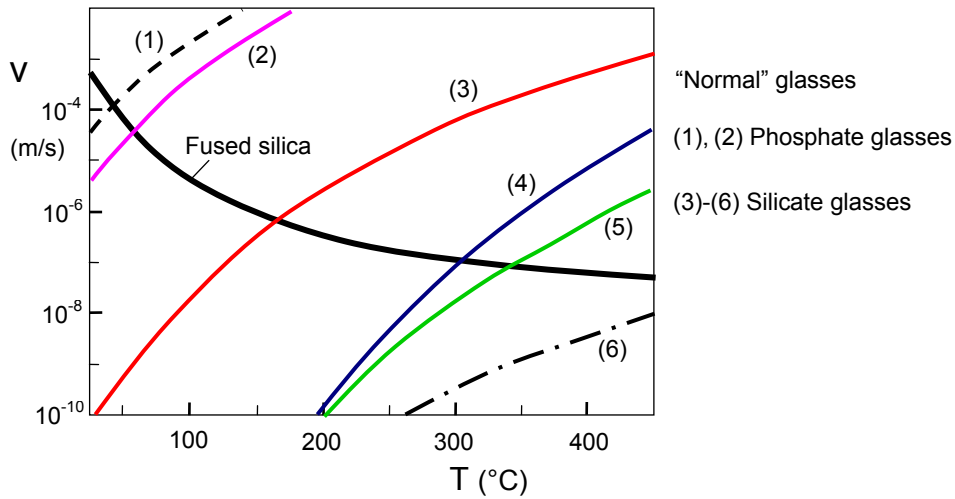
Fig. 1 Subcritical crack growth rate vs. temperature of different glasses for an individual stress intensity factor K=0.8 K_{IC}. Measurements in N_2 at 2700 Pa water vapour pressure except curves (3-6): measurements in vacuum [2]. Curves (1,2): Phosphate glasses. [8, 9]. Details can be found in [7].

2 Experimental results from literature

2.1 Crack-growth in water vapour

In order to discuss anomalous crack growth, some basic results from literature are compiled.

In Fig. 2a v-K-curves for constant vapour pressure of p=2100-2200 Pa and in Fig. 2b for 6.9-10 kPa are plotted [7]. There is a clear decrease of crack velocity with temperature visible. In contrast to the pressure influence, this behaviour had not been expected a priori and is the rea-son for the notation "anomalous subcritical crack growth".
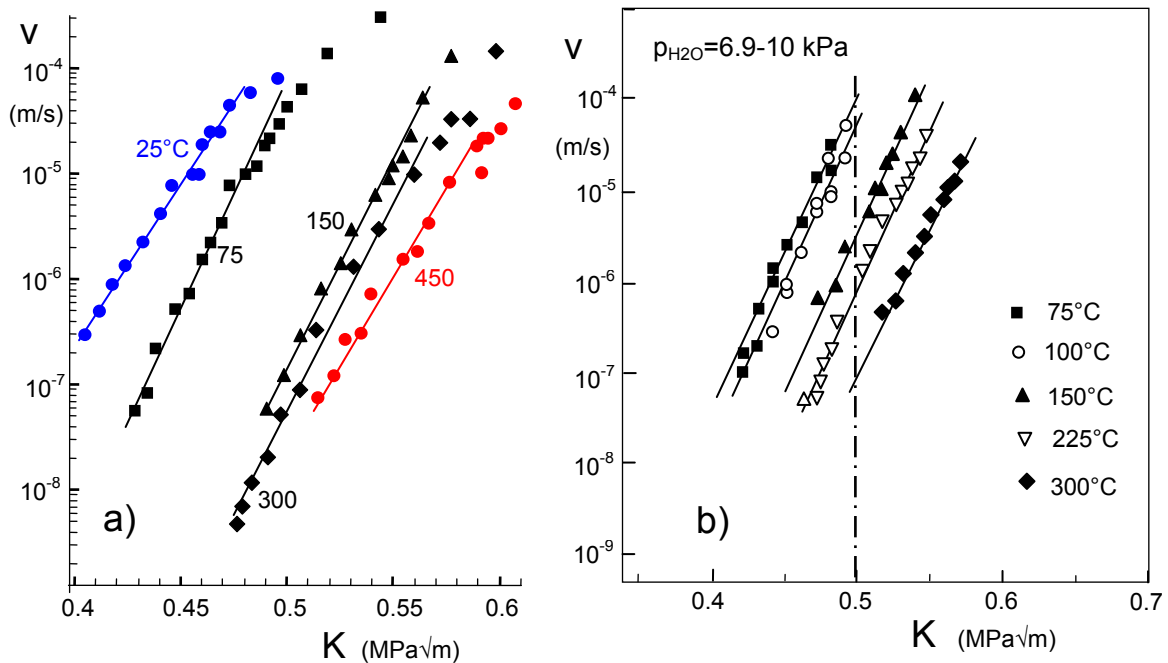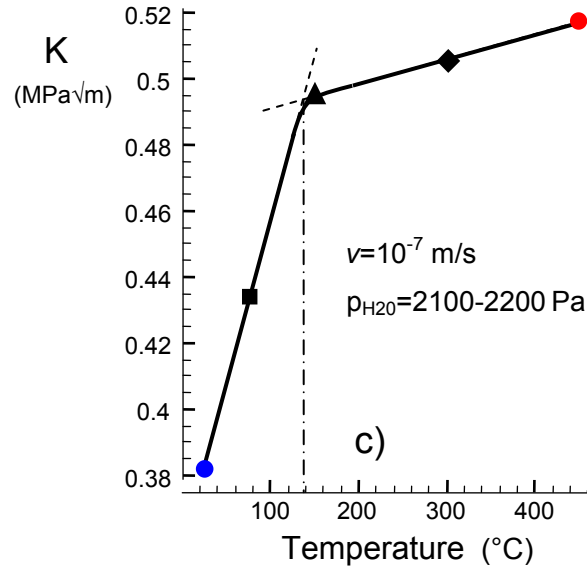
Fig. 2 v-K-curves for constant vapour pressure of a) p=2100-2200 Pa and b) 6900-10000 Pa by Suratwala and Steele [7], c) stress intensity factors necessary for a crack-growth rate of v=10^{-7}m/s at p=2100-2200 Pa pressure.

Finally, Fig. 2c shows the stress intensity factor necessary to reach a crack velocity of v=10^{-7} m/s at a partial water vapour pressure of p_{H2O}=2100-2200 as a function of temperature. There seems a change of the crack-growth behaviour visible at about 140°C.

2.2 Measurements in liquid water

Measurements on silica in liquid water were published by Wiederhorn and Bolz [1] as shown in Fig. 3a for the temperature region 2°C≤T≤90°C. This set of curves war fitted in [1] by the relation

$$v = v_0 \exp\left[\frac{-Q + bK}{RT}\right]$$
(4)

with the parameters ln(v_0)=-1.32±0.6 (v_0 in m/s), Q=139 kJ/mol, and b≅0.216±0.006 (in mks units). The dashed line was interpolated for comparisons with the results by Suratwala and Steele [7].

Since the v-K-curves should depend on the water concentrations at the glass surface, results of water concentrations are given in Fig. 3b in a semi-logarithmic plot as a function of temperature. These data represent the total water content C_w measured by Zouine et al. [10] under satu-ration pressure (open circles).

Silica reacts with the silica network according to

$$\equiv\text{Si-O-Si}\equiv + \text{H}_2\text{O} \leftrightarrow \equiv\text{SiOH} + \text{HOSi}\equiv$$
(5)

with the concentration of the hydroxyl S=[≡SiOH] and that of the molecular water C=[H_2O]. In *molar units*, the total water concentration C_w is given by

$$C_w = C + \tfrac{1}{2}S = C(1 + \tfrac{1}{2}k)$$
(6)

3

where k is the equilibrium constant describing the ratio of $k=S/C$.

A relation for the ratio of the two water species S/C, where S stands for the hydroxyl concentration and C for the concentration of molecular water, was given by Wiederhorn et al. [11]. For the temperature range of $90°C \leq T \leq 350°C$ the data are fitted by the straight line

$$k = \frac{S}{C} = A \exp\left(-\frac{Q}{RT}\right) \qquad (7)$$

(A=32.3 and Q=10.75 kJ/mol). The parabolic curves on each side of the straight line are the 95% confidence limits of the fit. Equations (6) and (7) result in

$$C = \frac{C_w}{1 + \frac{1}{2}k}, \qquad (8)$$

$$S = \frac{C_w}{\left(\frac{1}{2} + \frac{1}{k}\right)} \qquad (9)$$

and in *mass units*

$$S = \frac{17}{18} \frac{C_w}{\left(\frac{1}{2} + \frac{1}{k}\right)} \qquad (9a)$$

(the ratio 17/18 reflects the different mole masses of water and hydroxyl).
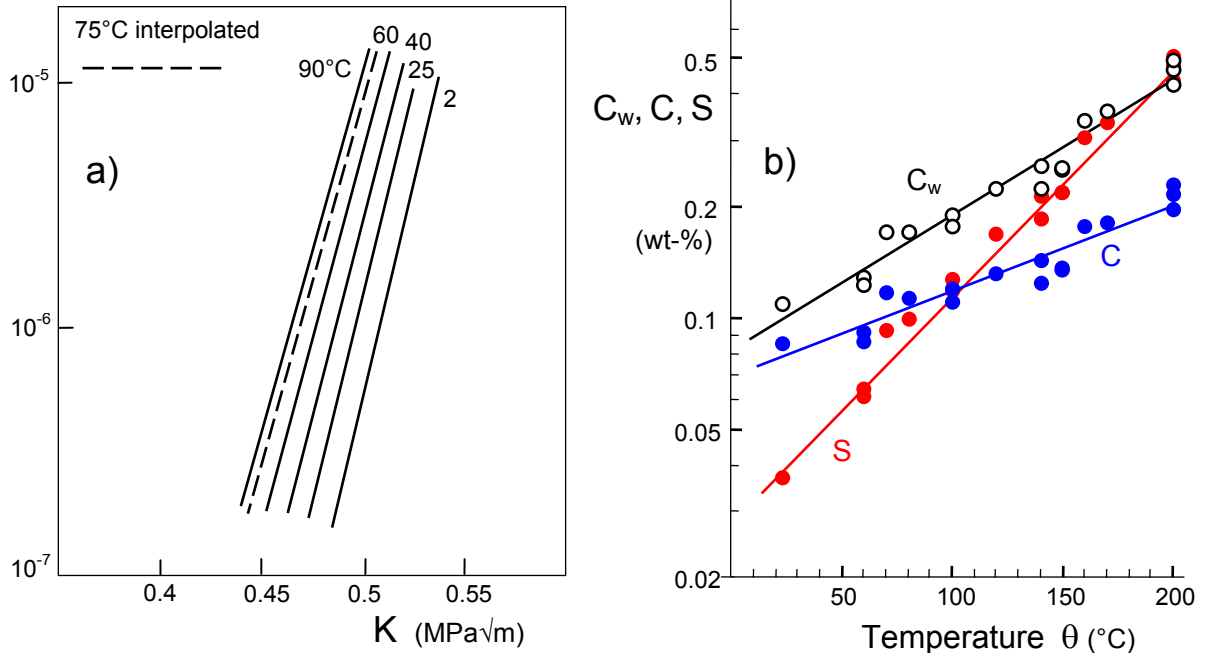

Fig. 3 a) v-K-curves for silica in liquid water by Wiederhorn and Bolz [1], b) solubility of water C_w at silica surfaces under saturation pressure derived from data by Zouine et al. [10], water species S and C.

4

In a rough representation by straight lines, the saturation-pressure data of Fig. 3b are given as

$$C_w = 0.000815 \exp(0.00839\,\theta) \tag{10}$$

$$S_{sat} \approx 0.000276 \exp(0.014\,\theta) \tag{11}$$

$$C \approx 0.000692 \exp(0.0053\,\theta) \tag{12}$$

3 *v-K*-curves for constant vapour pressure

The effect of water vapour pressure on the v-K-curves is clearly visible from Fig. 2. The crack-growth rates decrease with increasing temperature. At first glance, this seems to be in contrast to the results of Wiederhorn and Bolz [1], who found a higher cracking rate at elevated temperature, Fig. 3a. For the curves in Fig. 2a and 2b, however, it must be taken into account that the curves also show an increased saturation pressure when the temperature increases.

In order to eliminate this pressure influence, the curves of Fig. 3a were converted to common saturation pressure $p = 3.2$ kPa, the saturation pressure at 25° C, assuming Eq. (1). The result is plotted in Fig. 4. It can be seen that also with this representation a clear decrease of the crack velocity occurs with increasing temperature, so there is no discrepancy to the results of Suratwala and Steele [7].
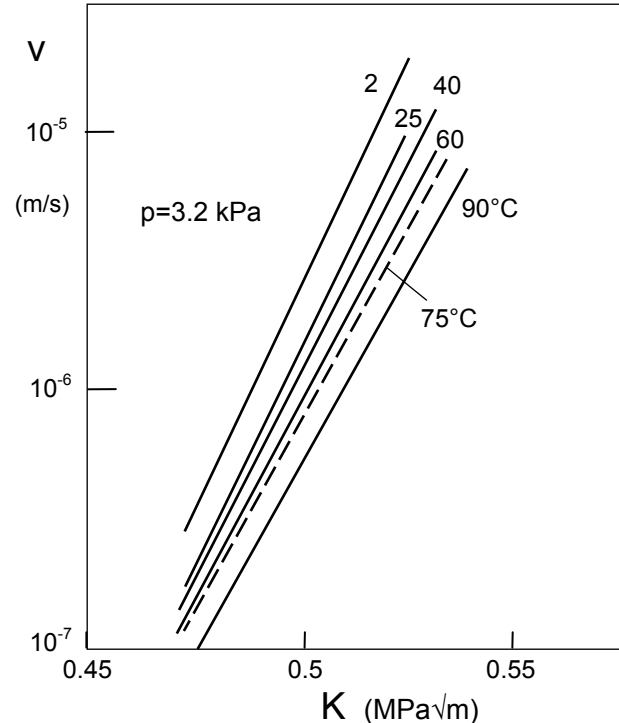

Fig. 4 v-K-curves for constant water vapor pressure, results by Wiederhorn and Bolz [1] transformed to a common saturation pressure of 3.2 kPa occurring as the saturation pressure at 25°C.

4 Hydroxyl and molecular water

The hydroxyl water at the water pressure of 355 Torr is shown in Fig. 5b. In contrast to Fig. 3b, the surface concentrations of Fig. 5a decrease with increasing temperature.

The data in Fig. 5a can be represented by straight lines for $1/T > 0.0022/K$:

$$C_{355\,Torr} \cong \exp\left[\underbrace{-18.94}_{A_1} + \frac{\overbrace{35.84\,kJ/mol}^{A_2}}{RT}\right] \qquad (13)$$

and

$$S_{355\,Torr} \cong \exp\left[-15.56 + \frac{25.09\,kJ/mol}{RT}\right] \qquad (14)$$

In [12] Davis and Tomozawa reported water concentrations that increase in the temperature region $\theta < 500°C$ as shown in Fig. 5b by the squares. These data may not be in equilibrium, as indicated already in [1]. To describe the data points, the relationship

$$S_{355\,Torr} \cong 0.533\exp\left[-\frac{34.3\,kJ/mol}{RT}\right] + 6.66\times10^{-8}\exp\left[\frac{28.0\,kJ/mol}{RT}\right] \qquad (15)$$

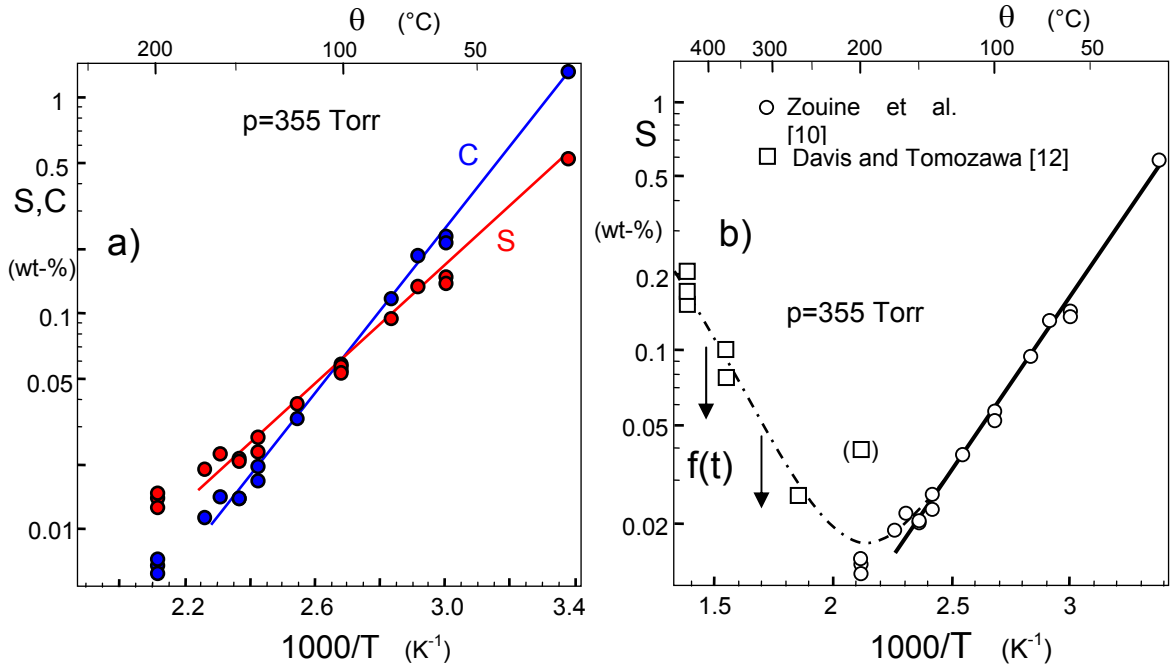would be appropriate. However, we do not want to make use of it.

Fig. 5 a) Concentrations of molecular and hydroxyl water from Fig. 3b, normalized on a constant water vapour pressure of $p = 355$ Torr, basic data from Zouine et al. [10], b) results for hydroxyl by Davis and Tomozawa [12] included (squares).

For the molecular water at a silica surface, Doremus [13] suggested the dependency

$$\Rightarrow C_{(mol)} \cong 0.015 \frac{p}{RT} \qquad (16)$$

where $C_{(mol)}$ is the concentration in molar units. Regarding this relation as a lower bound solution, we may use for the concentration in mass units

$$\Rightarrow C_{(mass)} \cong \frac{p}{355\,\mathrm{Torr}} \left(\exp\left[A_1 + \frac{A_2}{RT} \right] + \frac{A_3}{T} \right) \qquad (17)$$

with $A_3 = 6.87 \times 10^{-4}$ (°K) and the coefficients A_1 and A_2 given by eq.(13). The extrapolated concentration vs. temperature curve is plotted in Fig. 6 as the solid curve.
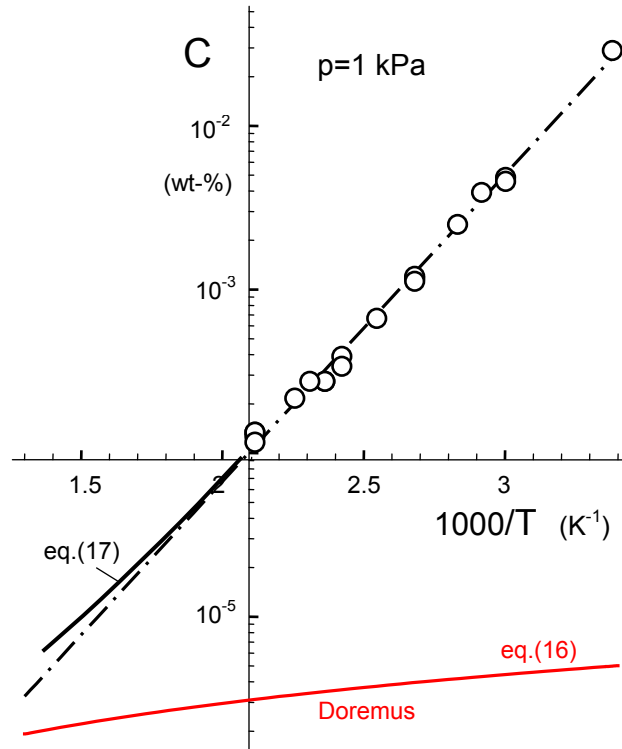
Fig. 6 Concentration of molecular water for p=1kPa water vapour pressure. Circles: computed from data by Zouine et al. [10], dash-dotted line: linear fit of the experimental data by eq.(13), red curve: suggestion by Doremus [13] for high temperatures, solid line: eq.(17).

The crack velocities are plotted in Fig. 7 in a normalized representation as v/C vs. K for the partial water vapour pressure of p=2.2 kPa. It can be seen that the total "scatter" of the v-K curves is strongly reduced compared with those of Fig. 2a.

Fig. 7 Crack-growth rates normalized on the molecular water concentration.

5 Computation of shielding stress intensity factor

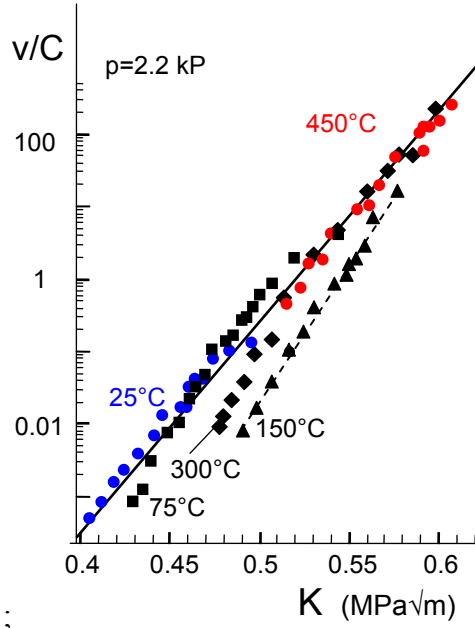In our opinion, at least a part of the observed trend is caused by crack-tip shielding. In the preceding considerations we implicitly identified the externally applied stress intensity factor K_{appl} with the K-value acting at the crack tip, K_{tip}. It was early outlined in [14,15] that a shielding stress intensity factor must develop as a consequence of volume increase by the hydroxyl generation (for references see e.g. [16]).

It has been shown in [17] that water-induced swelling at crack tips generates an intrinsic stress intensity factor $K_{sh}<0$ that shields a crack from an externally applied loading K_{appl} so that the stress intensity factor K_{tip} at the crack tip is reduced. The effective stress intensity factor acting at the crack tip, $K_{tip,}$ represents the singular stress field at the tip. From the principle of superposition, K_{tip} is given by

$$K_{tip} = K_{appl} + K_{sh} \tag{18}$$

i.e. $K_{tip}<K_{appl}$. The shielding stress intensity factor as a function of K_{tip} and rate v can be approximately written

$$K_{sh} = -0.209 \frac{\varepsilon_0 E}{1-\nu} \frac{\kappa}{\mathrm{PLog}\left[\frac{4p^2}{\sqrt{0.9}} \kappa \sqrt{\frac{v}{D_0}}\right]} \tag{19}$$

with the *product logarithm* or Lambert W function PLog, i.e. the solution $W = \mathrm{PLog}(z)$ of the equation $z=W \exp(W)$ (see e.g. [18]). The quantity, ε_0 is the volumetric swelling strain at the tip, E is Young's modulus, ν Poisson's ratio and D_0 the diffusivity in the absence of stresses. The abbreviation κ is given by

$$\kappa = \frac{(1+\nu)}{3} \frac{K_{tip}}{\sqrt{2\pi}} \frac{\Delta V_w}{RT} \tag{20}$$

8

with the activation volume ΔV_w for stress-enhanced water diffusion of roughly $\Delta V_w = 15$ cm^3/mol, the absolute temperature T(°K) and the gas constant R. The other abbreviations p and q are

$$p \cong 0.45 \exp(0.13\lambda) \ , \quad q = 0.225 \ . \tag{21}$$

$$\lambda = 0.19 \frac{\varepsilon_0 E}{(1-\nu)} \frac{\Delta V_w}{RT} \tag{22}$$

The temperature dependent *effective* diffusivity D_0 under saturation pressure and in absence of stresses is described by

$$D_{eff}(T) = A_0 \exp(-Q/RT) \tag{23}$$

with the activation energy Q. For the diffusion of water the results by Zouine et al. [10] may be used yielding in Q=72.3 kJ/mol, $\log_{10} A_0 = -8.12$ (A_0 in cm^2/s) for the *effective* diffusivity (temperature range 0°C to 200°C).

Under reduced pressure, the effective diffusivity reads according to [13, 19]

$$D_{eff} = \frac{D_{mw}}{\frac{1}{2} k + 1} \tag{24}$$

with the diffusivity D_{mw} for <u>m</u>olecular <u>w</u>ater and k according to eq.(7). Again from Zouine et al. [10] we obtain

$$D_{mw}(T) = A_1 \exp(-Q_1/RT) \tag{25}$$

with now Q=71.2 kJ/mol, $\log_{10} A_1 = -3.78$ (for A_1 in cm^2/s).

The volume swelling strain at the surface, ε_0, at room temperature was determined in two different ways. On the one hand, the deformations caused by the swelling on the fracture surface were measured by AFM [14,17]. This led to ε_0=0.13. On the other hand, measurements of the water content at crack tips [20] showed a total water content of 6.8 wt%. Under the assumption that only hydroxyl is present under the high stresses at crack tips, this leads to S=0.128 wt% corresponding to ε_0=0.125. Therefore, the value ε_0=0.13 was used in [14,17].

6 Discussion

6.1 Prediction of the $v(K_{tip})$-curves

The principal effect of temperature is schematically illustrated in Fig. 8a for two temperatures $T_2 > T_1$ at which normal subcritical crack growth may appear in a $v(K_{tip})$-representation. Normal subcritical crack growth behaviour may be assumed. Consequently, the crack-growth rate is higher at the higher temperature, $v_2 > v_1$, both at the same crack-tip stress intensity factor K_{tip}. On the other hand, we see from Figs. 3 that for the chosen parameters the shielding stress intensity factor by swelling increases with temperature, too. This is indicated in Fig. 8b by the differently long horizontal arrows. In cases where the shielding stress intensity factor at the higher temperature is sufficiently stronger, $|K_{sh2}| > |K_{sh1}|$, the crack-growth curve at the higher

9

temperature, $v(K_{appl})_2$, lies right from that for the lower temperature $v(K_{appl})_1$, indicating a negative temperature dependence.

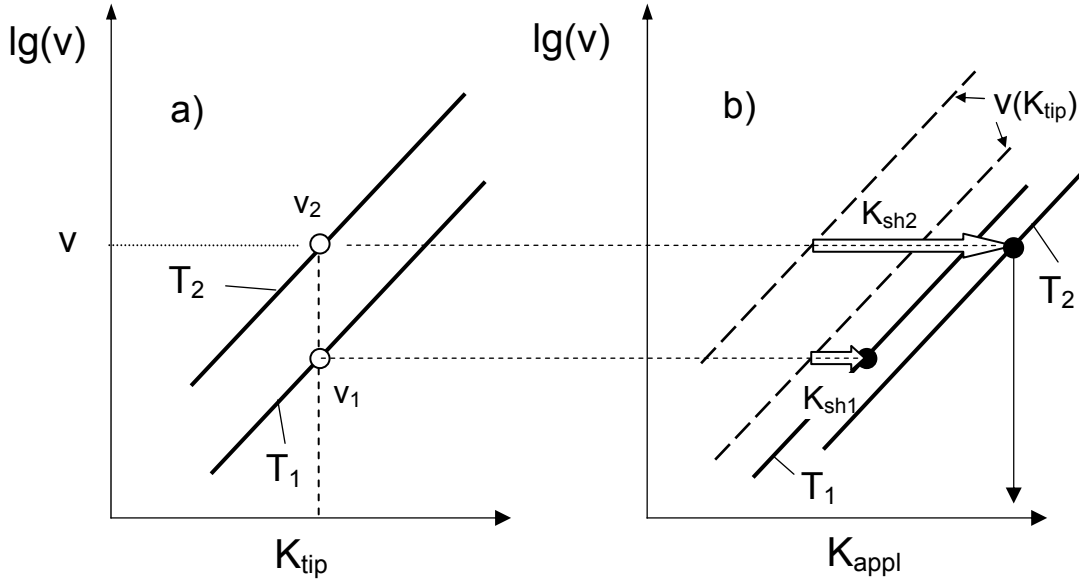**Fig. 8** Schematic of the temperature effect on the subcritical crack growth curves in different representations, a) $v(K_{tip})$, b) $v(K_{appl})$ obtained by temperature-dependent shielding terms K_{sh}.

The subcritical crack growth ratesof Fig. 7 are again plotted in Fig. 9a vs. the crack-tip stress in-tensity factor K_{tip}. It is clearly visible that the crack rates increase for constant K_{tip} with tem-perature and the slopes B of the curves decrease as is shown in Fig. 9b. The curves in Fig. 9a confirm the theoretical expectations from eqs.(1-4). For the slopes one expects:

$$\log v \propto BK_{tip}, \quad B = \frac{b}{RT} \tag{26}$$

i.e. a decrease with increasing reciprocal absolute temperature T. However, the $1/RT$-dependency is not exactly fulfilled. This is illustrated in Fig. 9c where the parameter b from eq.(26) is plotted. This quantity is not a constant but varies slightly between $b=0.18$ m$^{5/2}$/mol and $b=0.24$ m$^{5/2}$/mol. Nevertheless, this range is in good agreement with the result by Wiederhorn an Bolz [1] of $b=0.216\pm0.006$ m$^{5/2}$/mol. This result is included in Fig. 9c as the dash-dotted line with the related scatter band.

The parameter b is rather insensitive with respect to special choice of activation volume ΔV_w and the volume strain ε_0. This had been shown by Wiederhorn et al. [17] and is given here by Fig. 9d depending on ε_0 and ΔV_w. It can be concluded that in the range $5\% < \varepsilon_0 < 15\%$ the value b is about $b=0.204\pm0.06$ m$^{5/2}$/mol (hatched area), rather independent of the activation volume ΔV_w.

The slight temperature dependence of the data in Fig. 9c seems to be an indication for the fact that the shielding stress intensity factors reflecting only the effect of stress-enhanced diffusivity was considered in the model from [15,17]. Additional effects, namely stress-enhanced

swelling and material damage by hydroxyl generation in the crack-tip region should be included into the computations. Unfortunately, there is not yet a model available and has to be developed for this purpose.
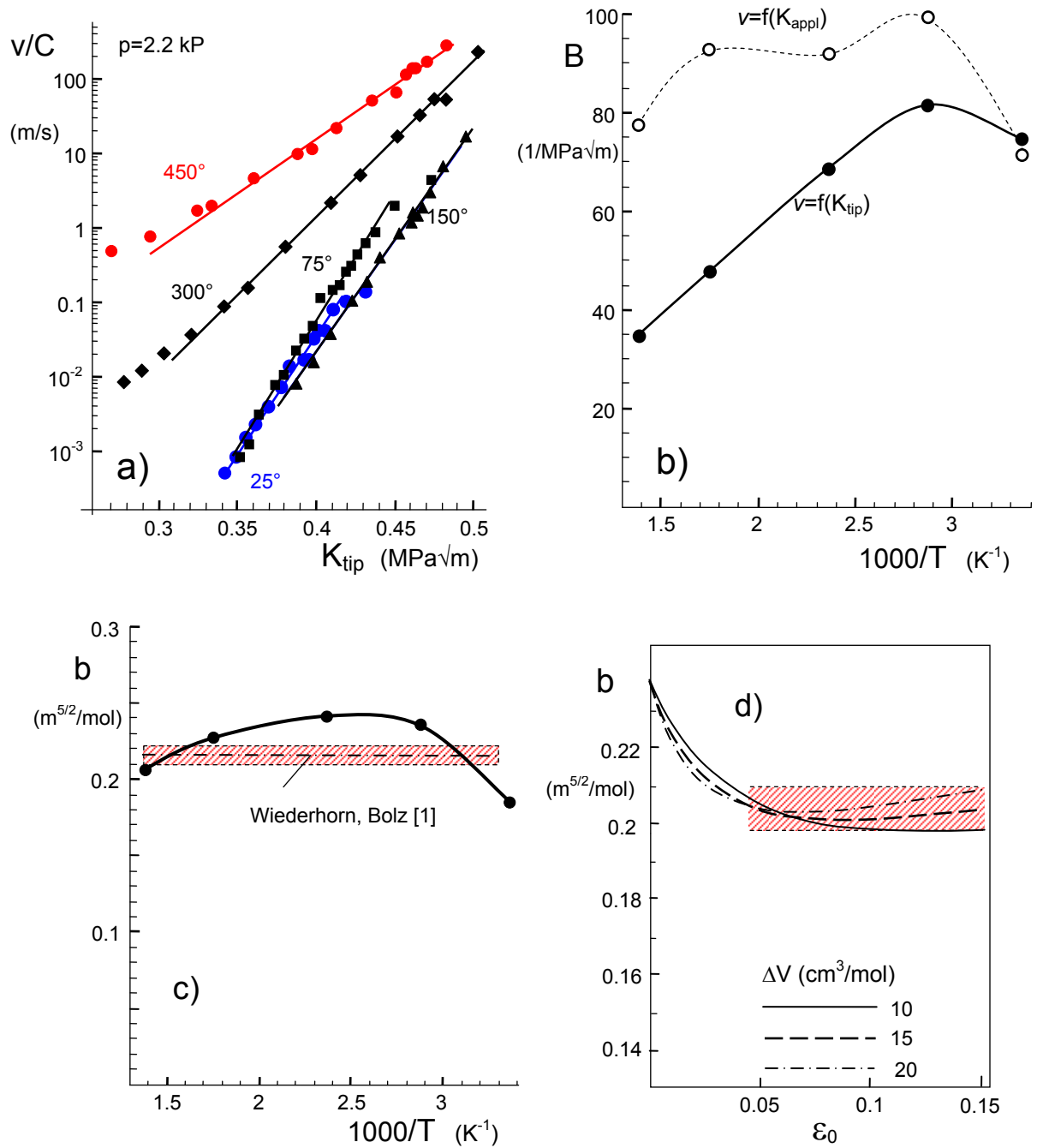

Fig. 9 a) Crack growth rates from Fig. 7 as a function of K_{tip}. b) Slopes of the individual straight lines in a) vs. reciprocal absolute temperature as solid symbols, open circles: slopes from Fig. 7, c) crack-growth parameter b from eqs.(1), (2), and (26), d) parameter b as a function of ε_0 and ΔV_w from Wiederhorn et al. [17].

11

6.2 Expectations for other glasses

In the previous considerations, only silica was considered. In this Section, we will look on other glasses, too. Density measurements on several glass compositions were reported by Scholze [21]. The materials were: (B) B_2O_3-glass, (K) K_2O-SiO_2-glass (20-80 mol-%), (Ca) Na_2O-CaO-SiO_2-glass (16-10-74 mol-%), (Al) Li_2O-Al_2O_3-SiO_2-glass (20-5-75 mol-%), and (Si) silica. The relative density changes due to water content C_w are given in Fig. 10a. Whereas for silica a non-linear behaviour $\Delta\rho(C_w)$ is reported in [21], for all other glasses straight-line behaviour was found. It has to be taken into account that the data scatter for silica is rather large as the data reported by Shelby [16] show which are introduced in red. The straight line represents the average of data for *as-received* water in silica measured by several authors and quoted by Shelby [16]. The circles are results by Brückner [22] measured by *water removal* (also quoted in [16]).

Whereas silica shows a density decrease with increasing water content, the densities of the other glasses increased with increasing C_w.

The relative density changes $\Delta\rho/\rho_0$ were transformed into volume strains ε_v. via

$$V = \frac{m}{\rho} \ \Rightarrow \ \varepsilon_v = \frac{\Delta V}{V} = \frac{\Delta m}{m} - \frac{\Delta\rho}{\rho}, \quad \Delta m = m_w = C_w m \qquad (27)$$

The results are plotted in Fig. 10b and compiled in Table 1.

Whereas the B_2O_3-glass shows strong volume shrinking due to water uptake, silica shows clear volume expansion. The effects on the other glasses are rather small. Materials Ca and Al also swell. *K* shrinks slightly.

In contrast to the crack-tip shielding for silica, it has to be expected that the borosilicate glass B should exhibit an increase of total stress intensity factors. Slight shielding effects may occur in the soda-lime glass as well as in the Al-glass.

Glass	Composition (mol-%)	(wt-%)	ρ_0 (g/cm^3)	$\dfrac{\Delta\rho}{\rho_0 C_w}$	ε_v/C_w, eq.(27)
B	B_2O_3-glass	-	1.83	6.3	−5.3
K	K_2O-SiO_2-glass (20-80)	(28.2-71.8)	2.38	1.41	−0.41
Ca	Na_2O-CaO-SiO_2-glass (16-10-74)	(16.6-9.4-74.1)	2.49	0.46	0.54
Al	Li_2O-Al_2O_3-SiO_2-glass (20-5-75)	(10.7-9.1-80.2)	2.33	0.37	0.63
Si	SiO_2	-	2.2	−0.84	1.84

Table 1 Swelling and shrinking strains derived from density curves given by Scholze [21].

The swelling effect is evident also from quantum mechanical computations by Zhu et al. [23]. These authors made quantum mechanics computations on a SiO_2-nanorod of 36 SiO_2 atoms to which they added a single water molecule.
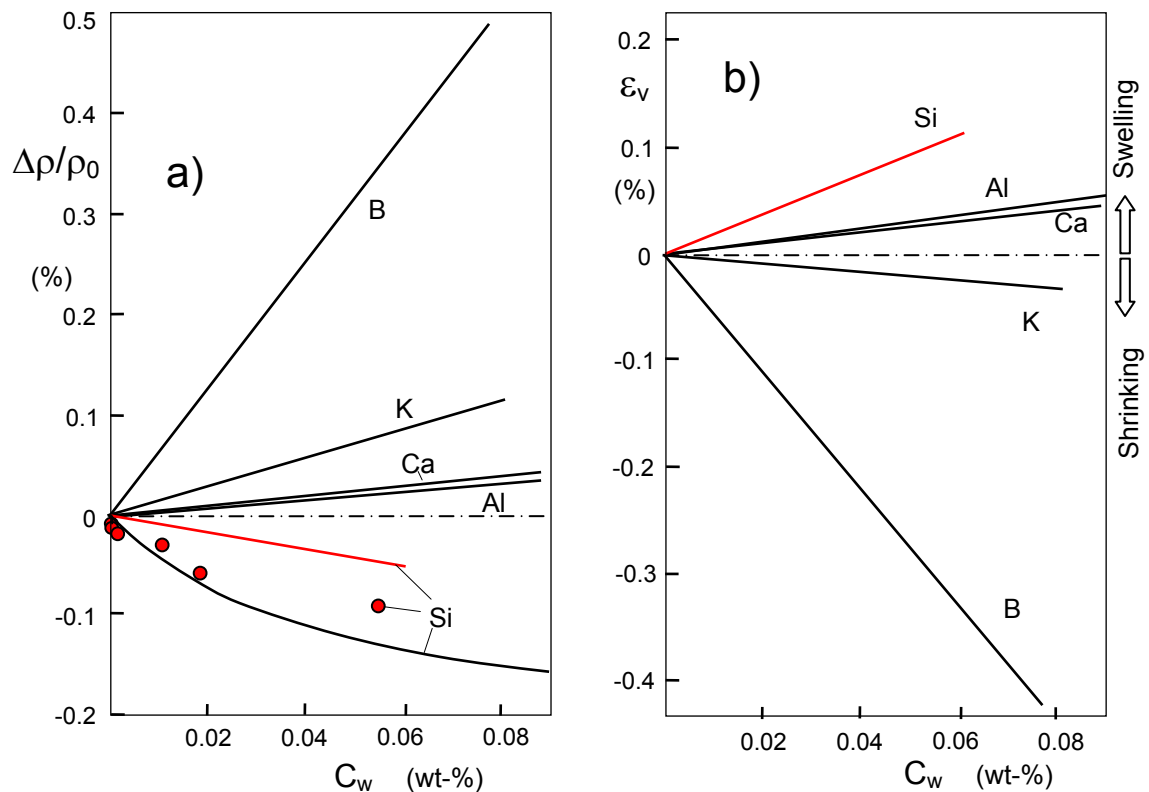
Fig. 10 a) Density change of glasses as a function of water content. Black curves given by Scholze [21], red line: average of data for as-received water in silica quoted by Shelby [16], circles: data from Brückner for water removal, also quoted in [22]. B: B_2O_3-glass, K: K_2O-SiO_2-glass (20-80 mol-%), Ca: Na_2O-CaO-SiO_2-glass (16-10-74 mol-%), Al: Li_2O-Al_2O_3-SiO_2-glass (20-5-75 mol-%); b) volume strains computed from Fig. 10a.

References

1. S.M. Wiederhorn and L.H. Bolz, "Stress Corrosion and Static Fatigue of Glass," *J. Am. Ceram. Soc.* **53**[10] 543-548 (1970).

2. S.M. Wiederhorn, H. Johnson, A.M. Diness and A.H. Heuer, "Fracture of Glass in Vacuum," *J. Am. Ceram. Soc.* **57** [8] 336-341 (1974).

3. S. Sakaguchi and Y. Hibino,"Fatigue in low-strength silica optical fibres," *J. Mater. Sci.* **19** 3416-3420 (1984).

4. M. Muraoka and H. Abé, "Subcritical Crack Growth in silica Optical Fibers in a Wide Range of Crack Velocities," *J. Am. Ceram. Soc.* **79**[1] 51-57 (1996).

5 Wiederhorn, S.M., Influence of water vapour on crack propagation in soda-lime glass, J. Am. Ceram. Soc. **50**(1967), 407-414.

6 S.M. Wiederhorn, E.R. Fuller, R. Thomson, Micromechanisms of crack growth in ceramics and glasses in corrosive environments, Metal Science, Aug-Sept (1980), 450-458.

7 T.I. Suratwala and R.A. Steele, "Anomalous temperature dependence of sub-critical crack growth in silica glass," *J. Non-Crystalline Sol.* **316** 174-182 (2003).

8 T.I. Suratwala, R.A. Steele, G.D. Wilke, J. Campbell, *J. Non-Crystalline Sol.* **263/264**(2000), 213.

9 S. Crichton, M. Tomozawa, J. Hayden, T. Suratwala, J. Campbell, *J. Am. Ceram. Soc.* **82** (1999), 3097.

10 A. Zouine, O. Dersch, G. Walter and F. Rauch, "Diffusivity and solubility of water in silica glass in the temperature range 23-200°C," *Phys. Chem. Glass: Eur. J. Glass Sci and Tech. Pt. B*, **48** [2] (2007), 85-91.

11 S. M. Wiederhorn, F. Yi, D. LaVan, T. Fett, M.J. Hoffmann, Volume Expansion caused by Water Penetration into Silica Glass, *J. Am. Ceram. Soc.* **98** (2015), 78-87.

12 Davis, K.M., Tomozawa, M., Water diffusion into silica glass: structural changes in silica glass and their effect on water solubility and diffusivity, J. Non-Cryst. Sol. **185** (1995), 203-220.

13 R.H. Doremus, Diffusion of Reactive Molecules in Solids and Melts, Wiley, 2002, New York.

14 S. M. Wiederhorn, T. Fett, G. Rizzi, S. Fünfschilling, M.J. Hoffmann, J.-P. Guin, Effect of Water Penetration on the Strength and Toughness of Silica Glass, J. Am. Ceram. Soc. **94** [S1] (2011), 196-S203.

15 S.M. Wiederhorn, T. Fett, G. Rizzi, M. Hoffmann, J.-P. Guin, "Water Penetration – its Effect on the Strength and Toughness of Silica Glass," *Met. Mater. Trans. A*, **44**(2013) [3], 1164 -1174.

16 Shelby, J.E., "Density of vitreous silica," J. Non-Cryst. **349** (2004), 331-336.

17 Wiederhorn, S.M., Fett, T., Rizzi, G., Hoffmann, M.J., Guin, J.-P., The Effect of Water Penetration on Crack Growth in Silica Glass, Engng. Fract. Mech., **100** (2013), 3–16.

18 R. Corless, G. Gonnet, D. Hare, D. Jeffrey and D. Knuth, "On the Lambert W Function," Advances in Computational Mathematics, **5**(1996), 329-359.

19 Oehler, A., Tomozawa, M., Water diffusion into silica glass at a low temperature under high water vapor pressure, J. Non-Cryst. Sol. **347** (2004) 211-219.

20 M. Tomozawa, W.-T. Han and W.A. Lanford, "Water Entry into Silica Glass during Slow Crack Growth," J. Am. Ceram. Soc. **74** [10] (1991) 2573-2576.

21 Scholze, H., Glas, Springer Verlag, Berlin, 1988.

22 Brückner, R., "Metastable equilibrium density of hydroxyl-free synthetic vitreous silica," J. Non-Cryst. Solids, **5** (1971), 281-5

23 T. Zhu, J. Li, X. Lin, S. Yip, Stress-dependent molecular pathways of silica-water reaction, J. of Mechanics and Physics of solids, **53**(2005), 1597-1623.

www.kit.edu